



MIT Open Access Articles

Understanding of the contact of nanostructured thermoelectric n-type Bi₂Te_{2.7}Se_{0.3} legs for power generation applications

The MIT Faculty has made this article openly available. **Please share** how this access benefits you. Your story matters.

Citation	Liu, Weishu, Hengzhi Wang, Lijuan Wang, Xiaowei Wang, Giri Joshi, Gang Chen, and Zhifeng Ren. "Understanding of the Contact of Nanostructured Thermoelectric n-Type Bi ₂ Te _{2.7} Se _{0.3} Legs for Power Generation Applications." J. Mater. Chem. A 1, no. 42 (2013): 13093.
As Published	http://dx.doi.org/10.1039/c3ta13456c
Publisher	Royal Society of Chemistry
Version	Author's final manuscript
Citable link	http://hdl.handle.net/1721.1/89470
Terms of Use	Creative Commons Attribution-Noncommercial-Share Alike
Detailed Terms	http://creativecommons.org/licenses/by-nc-sa/4.0/

Understanding of the contact of nanostructured thermoelectric n-type $\text{Bi}_2\text{Te}_{2.7}\text{Se}_{0.3}$ legs for power generation applications

Weishu Liu,^{*a} Hengzhi Wang,^{*b} Lijuan Wang,^{a,c} Xiaowei Wang,^c Giri Joshi,^c Gang Chen^{§d} and Zhifeng Ren^{§a}

^a Department of Physics and TcSUH, University of Houston, Houston, Texas 77204, USA.

^b Department of Physics, Boston College, Chestnut Hill, Massachusetts 02467, USA

^c GMZ energy, Waltham, Massachusetts 02458, USA

^d Department of Mechanical Engineering, Massachusetts Institute of Technology, Cambridge, Massachusetts 02139, USA.

^e School of Science, Minzu University of China, Beijing, 100081, China

* Equal contribution

§ Prof. Chen, E-mail: gchen2@mit.edu; Fax: +1-617-324-5519; Tel: +1-617-253-0006. Prof. Ren, E-mail: zren@uh.edu; Fax: +1-713-743-8201, Tel: +1-713-743-8217

Abstract

Traditional processes of making contacts (metallization layer) onto bulk crystalline Bi_2Te_3 -based materials do not work for nanostructured thermoelectric materials because of either weak bonding strength or unstable contact interface under temperature higher than 200 °C. Hot pressing of nickel contact onto the nanostructured thermoelectric legs in a one-step process leads to strong bonding. However, such process caused a large contact resistance in n-type $\text{Ni}/\text{Bi}_2\text{Te}_{2.7}\text{Se}_{0.3}/\text{Ni}$ legs, although not in p-type $\text{Ni}/\text{Bi}_{0.4}\text{Sb}_{1.6}\text{Te}_3/\text{Ni}$ legs. A systematic study was carried out to investigate the detailed reaction and diffusion at the interface of the nickel layer and n-type Bi_2Te_3 -based thermoelectric material layer. We found that a p-type region formed within the n-type $\text{Bi}_2\text{Te}_{2.7}\text{Se}_{0.3}$ during hot pressing due to Te deficiency and Ni doping, leading to the large contact resistance.

1. Introduction

Thermoelectric (TE) power generators, which have been used to provide electrical power for space vehicles,¹ now are considered for waste heat and solar energy harvesting into electricity.^{2,3} Bi₂Te₃ and its alloys with Sb₂Te₃ and Bi₂Se₃ are well known for their good thermoelectric performance near room temperature.^{4,5} Progress by nanostructure engineering has further improved their performance.⁶⁻¹³ Recently, a flat-panel solar thermoelectric power generator, using high thermal concentration of ~300 but no optical concentration to maintain a hot side at 220 °C and cold side at 20 °C, achieved a system efficiency of 4.6%.^{14,15} The metallization layer (nickel) made onto both the n- and p-type nanostructured legs for this concept-proof STEG device were by sputtering method.^{14,15} However, sputtering is not a scalable method for mass production of such devices operating at temperature above 200 °C, which require a thick nickel layer to prevent the Cu from the electrode^{16,17} and also Sn from solder diffusing into the thermoelectric materials^{18,19}. Electrochemical deposition process was used to make thicker nickel layer.^{19,20} However, the weak-bonding interface (<10 MPa), between the nickel and thermoelectric material, leads to severe device degradation. Since the power generation device operates at much higher temperature (~250 °C) and larger temperature gradient (100~200 °C mm⁻¹) than that of the cooling device (~50 °C and 20~30 °C mm⁻¹, respectively), stronger bonding strength is required between the Cu electrode and the thermoelectric elements.

In addition to the bonding strength, the electrical contact resistance between the electrode and thermoelectric materials needs to be minimized. The contact resistance R_c between the electrode and thermoelectric legs decreases the effective $\langle ZT \rangle_D$ of thermoelectric devices according to,²¹

$$\langle ZT \rangle_D = \frac{L}{L + 2R_c\sigma} \langle ZT \rangle_M, \quad (1)$$

where L is the length of the thermoelectric leg, R_c is the contact resistance, σ is the electrical conductivity of the thermoelectric leg, and $\langle ZT \rangle_M$ is the effective ZT of the thermoelectric material between T_h and T_c . For a typical device $L \sim 1$ mm, and $\sigma \sim 10^5$ S m⁻¹, R_c should be much less than $L/2\sigma \sim 10^{-8}$ Ω m² (10^{-4} Ω cm²). Ideally, the contact resistance should be less than 1 μΩ cm².

In order to achieve higher bonding strength at the Ni/TE interface, we directly pressed a Ni powder layer onto Bi₂Te₃ powder layer by hot pressing. A significantly improved bonding strength was obtained in both n-type Ni/Bi₂Te_{2.7}Se_{0.3} (~20 MPa) and p-type Ni/Bi_{0.4}Sb_{1.6}Te₃ (~30 MPa) legs. However, a very large contact resistance was observed in n-type Ni/Bi₂Te_{2.7}Se_{0.3} (~210 μΩ cm²) even though the contact resistance for p-type Ni/Bi_{0.4}Sb_{1.6}Te₃ is less than 1 μΩ cm², as illustrated in Fig. 1. The high contact resistance we observed should be related to the interface reaction of Ni/Bi₂Te_{2.7}Se_{0.3}.^{22,23} In this paper, we carried out detailed studies to investigate the cause of the large contact resistance at the interface of Ni/Bi₂Te_{2.7}Se_{0.3} formed by the direct current induced hot press process.

2. Experimental details

Synthesis of thermoelectric elements for the device. The elemental chunks were weighted according to the formula of Bi_{0.4}Sb_{1.6}Te₃ for p-type and Bi₂Te_{2.7}Se_{0.3} for n-type, and then subjected to ball milling. The ball milled powders were subsequently loaded into a graphite die and sintered by direct current induced hot pressing^{12,13}.

Synthesis of compounds for studying the interface reaction. Ball milling and hot pressing processes were also used to synthesize the possible compounds formed at the interface during hot pressing, including NiSe, NiTe, Ni₃Te₂, and Ni₂Te₃. In

order to investigate the doping effect of minor Ni in thermoelectric elements, $\text{Bi}_2\text{Te}_{2.7}\text{Se}_{0.29}\text{Ni}_{0.01}$, $\text{Ni}_{0.01}\text{Bi}_{1.99}\text{Te}_{2.7}\text{Se}_{0.3}$, and $\text{Ni}_{0.01}\text{Bi}_2\text{Te}_{2.7}\text{Se}_{0.3}$ were studied. Furthermore, more than 15 compounds with the general formula $(\text{Bi}_{1-x}\text{Ni}_x)_2(\text{Te, Se})_{3-\delta}$ were also synthesized to investigate the combined effect of the nickel doping and also the tellurium deficiency on the contact resistance.

Contact fabrication. For the hot-pressed contact, commercial Ni powders, $\text{Bi}_{0.4}\text{Sb}_{1.6}\text{Te}_3$, and $\text{Bi}_2\text{Te}_{2.7}\text{Se}_{0.3}$ nanopowders were loaded in a graphite die within a glove box under the argon protection, as followings: Ni/ $\text{Bi}_{0.4}\text{Sb}_{1.6}\text{Te}_3$ /Ni for the p-type leg, and Ni/ $\text{Bi}_2\text{Te}_{2.7}\text{Se}_{0.3}$ /Ni for the n-type leg. The graphite die was subsequently subjected to a hot pressing process.^{12, 13}

Structure characterization. X-ray diffraction (XRD) measurements were conducted on a PANalytical multipurpose diffractometer with an X'celerator detector (PANalytical X'Pert Pro).

Elemental composition measurement. The chemical composition analysis was carried out on the field emission scanning electron microscopy (SEM, JEOL-6340F) and transmission electron microscopy (TEM, JEOL-2010F).

Thermoelectric transport property measurements. The electrical resistivity was measured by a four-point method, while the Seebeck coefficient was determined by the slope of the voltage difference versus temperature difference curve based on a static temperature difference method. The simultaneous measurement of electrical resistivity and Seebeck coefficient was conducted on a commercial system (ZEM-3, ULVAC).

Measurement of contact resistance. The electrical contact resistance was measured from a scanning voltage probe, as shown in Fig. 1. Voltage drop along a TE element is measured as a small current passes through the element. A typical dimension of the sample for the contact resistance measurement is around 1.8 mm x 1.8 mm x 2.4 mm and a typical current used is 0.1 A.

Bonding strength measurement. The bonding strength is measured by the tensile strength test. The thermoelectric element with Ni layer (1.8 mm x 1.8 mm x 2.4 mm) was welded on aluminum holder by solder, and then subjected to the tensile strength test.

Fig. 2 shows the microstructure of the contact region (cross-section) between the Ni metallization layer and thermoelectric (TE) elements in both p-type leg Ni/ $\text{Bi}_{0.4}\text{Sb}_{1.6}\text{Te}_3$ /Ni and n-type leg Ni/ $\text{Bi}_2\text{Te}_{2.7}\text{Se}_{0.3}$ /Ni, which was made by directly hot pressing layered Ni powder and TE powders. A layer (gray region) between the Ni (dark region) and TE (light region) was clearly seen from both n-type and p-type legs, which could be a new product due to the interface reaction during hot pressing. Here, we refer it as an interface reaction layer (IRL). The thickness of the IRL in n-type leg ($\sim 4 \mu\text{m}$, hot pressed at 400 °C) is slightly thicker than that in p-type leg ($\sim 3 \mu\text{m}$, hot pressed at 400 °C). With the increased hot pressing temperature from 400 °C to 500 °C, the thickness of the IRL also increases from $\sim 3 \mu\text{m}$ to 13~16 μm for p-type leg, and from $\sim 4 \mu\text{m}$ to 17~21 μm for n-type. A selected area ($\sim 2 \times 20 \mu\text{m}^2$) SEM-EDS was conducted to detect the atomic composition profile crossing from Ni side to thermoelectric materials side, as shown in the Fig. 3. From the Ni concentration profile, it seems that a thicker Ni_3Te_2 and a thinner NiTe were formed at Ni/ $\text{Bi}_{0.4}\text{Sb}_{1.6}\text{Te}_3$ interface, while a thinner Ni_3Te_2 and a thicker NiTe were formed at Ni/ $\text{Bi}_2\text{Te}_{2.7}\text{Se}_{0.3}$ interface. After the IRL, a significantly thicker Te-deficient region (TDR) was observed in Ni/ $\text{Bi}_2\text{Te}_{2.7}\text{Se}_{0.3}$ samples, whereas stoichiometric $\text{Bi}_{0.4}\text{Sb}_{1.6}\text{Te}_3$ was observed right after the IRL in Ni/ $\text{Bi}_{0.4}\text{Sb}_{1.6}\text{Te}_3$. The formation of TDR suggested that the interfacial reaction consumes more chalcogen element in the n-type leg than that in the p-type leg.

To confirm the reaction product at the interface region, we mixed 20 wt.% Ni with 80 wt.% TE powders of both p- and n-type and hot pressed. The X-ray diffraction (XRD) patterns, shown in Fig. 4, clearly indicate that both the hexagonal nickel and rhombohedral Bi_2Te_3 -based materials were present, plus another phase that matches well with those of NiTe shown in Fig. 4(c). This is consistent with the observation by Lyore et al.,²³ in which a NiTe phase was observed by TEM in a Ni/ $\text{Bi}_2\text{Te}_{2.7}\text{Se}_{0.3}$ interface after annealing at 200 °C. In their work, the Ni layer was deposited onto $\text{Bi}_2\text{Te}_{2.7}\text{Se}_{0.3}$ by sputtering. The NiTe bulk, shown in Fig. 4(c), was made by ball milling and hot pressing. Furthermore, it is noted that the major impurity peaks in Fig. 4(b) have a slight larger 2θ than that of Fig. 4(a). More careful analysis of the XRD pattern of Fig. 4(b) shows that the impurity phase is more close to Ni_2SbTe ,²⁴ which has a similar hexagonal crystalline structure (P63/mmc, No. 194) with NiTe, but with Sb and Te sharing the same atomic site in the corresponding crystal structure. According to the chemical composition of the IRL of Ni/ $\text{Bi}_{0.4}\text{Sb}_{1.6}\text{Te}_3$ interface as shown in Fig. 3(a), the impurity phase should be $\text{NiTe}_{1-x}\text{Sb}_x$. In other words, both Te and Sb from $\text{Bi}_{0.4}\text{Sb}_{1.6}\text{Te}_3$ reacted with Ni at the Ni/ $\text{Bi}_{0.4}\text{Sb}_{1.6}\text{Te}_3$ interface, explaining no obvious Te deficiency in $\text{Bi}_{0.4}\text{Sb}_{1.6}\text{Te}_3$ shown in Fig. 3(a), but significant Te deficiency in $\text{Bi}_2\text{Te}_{2.7}\text{Se}_{0.3}$ shown in Fig. 3(b). However, Ni_3Te_2 did not show up in Fig. 4. According to the Ni-Te phase diagram, Ni_3Te_2 is also a stable phase when enough Ni exists. To find out whether Ni_3Te_2 phase forms at the interface, we synthesized NiTe by ball milling and sandwiched it between Ni and $\text{Bi}_2\text{Te}_{2.7}\text{Se}_{0.3}$ to form a new layer structure, i.e., Ni/NiTe/ $\text{Bi}_2\text{Te}_{2.7}\text{Se}_{0.3}$ /NiTe/Ni. The thickness is 0.3, 0.2, and 1.5 mm for Ni, NiTe, and $\text{Bi}_2\text{Te}_{2.7}\text{Se}_{0.3}$, respectively. After hot pressing, it is found that a new layer of Ni_3Te_2 was clearly formed from the reaction of $\text{Ni}+\text{NiTe}\rightarrow\text{Ni}_3\text{Te}_2$. The thickness of the newly formed Ni_3Te_2 is $\sim 100\ \mu\text{m}$. At the interface between NiTe and $\text{Bi}_2\text{Te}_{2.7}\text{Se}_{0.3}$, significant diffusion of Te from $\text{Bi}_2\text{Te}_{2.7}\text{Se}_{0.3}$ into the NiTe layer happened: $\text{NiTe}+\text{Bi}_2(\text{Te, Se})_3\rightarrow\text{NiTe}_{1+\delta}+\text{Bi}_2(\text{Te, Se})_{3-\delta}$, causing Te deficiency in $\text{Bi}_2\text{Te}_{2.7}\text{Se}_{0.3}$, as shown in Fig. 5. Thus, the NiTe layer is not an effective barrier layer to block the diffusion of Ni into the thermoelectric materials, which could be the reason for the efficiency degradation due to the unstable interface.

Another interesting observation from the selected area SEM-EDS is the diffusion of Ni in the Bi_2Te_3 -based materials. We noted an “abnormally” high concentration of Ni (2~7%) even 10~20 μm away from the IRL. Fig. 6 shows the typical TEM images and EDS compositions of selected points at the Ni/ $\text{Bi}_2\text{Te}_{2.7}\text{Se}_{0.3}$ interface. The thickness reduction was achieved from the thermoelectric material side slowly approaching the Ni side in the preparation of TEM sample. A boundary between the thermoelectric material and the IRL, characterized with some holes, are clearly seen from Fig. 6 (b). One special feature was the sharp tips near the Ni/ $\text{Bi}_2\text{Te}_{2.7}\text{Se}_{0.3}$ interface in the thermoelectric material side. The TEM-EDS suggested that most of this sharp tip composed of “abnormally” high concentration of Ni (>50 at.%), which was summarized in Fig. 6(a). A near pure Ni needle was found, as shown in Fig. 6(d), which could be a direct evidence of the fast diffusion of Ni along the $\text{Bi}_2\text{Te}_{2.7}\text{Se}_{0.3}$ grain boundary. A schematic model for the diffusion of Ni into $\text{Bi}_2\text{Te}_{2.7}\text{Se}_{0.3}$ was shown in Fig. 6(e). One possible explanation is that residual Ni is left at the interface during the thickness reduction process of the TEM sample because Ni is much harder than $\text{Bi}_2\text{Te}_{2.7}\text{Se}_{0.3}$. These Ni residuals would diffuse into $\text{Bi}_2\text{Te}_{2.7}\text{Se}_{0.3}$ further during the operation. Similar fast diffusion along grain boundary was also reported at the Cu/Bi interface.²⁵

4. The reasons for the high contact resistance

From the discussion in the above section, possible reasons causing the high contact resistance in n-type Ni/ $\text{Bi}_2\text{Te}_{2.7}\text{Se}_{0.3}$ /Ni legs made by direct hot pressing are probably 1) the poor electrical conductivity of the new reaction product, 2) the Te-deficient region, and 3) the carrier concentration change due to Ni diffusion into $\text{Bi}_2\text{Te}_{2.7}\text{Se}_{0.3}$. We further analyze these possible reasons below.

4.1 Effect of the new reaction product

Apart from the NiTe reaction product confirmed by the XRD pattern in section 3, other possible phases NiSe, Ni₂Te₃, and Ni₃Te₂ according to the Ni-Se and Ni-Te phase diagram, were also synthesized by the high-energy ball milling and hot pressing. Fig.7 shows their temperature dependent Seebeck coefficient and electrical resistivity. It is found that all the samples show a metal-like behavior with low electrical resistivity (0.5~0.6 μΩ m), which is slightly higher than that of hot pressed Ni at 500 °C (0.15 μΩ m, density = 6.2 g cm⁻³), but much lower than that of Bi₂Te_{2.7}Se_{0.3} (~10 μΩ m). Therefore the high contact resistance cannot be from the resistance of these reaction products. Furthermore, all the samples we investigated show a negative Seebeck coefficient (-5 to -15 μV K⁻¹), of the same type as Bi₂Te_{2.7}Se_{0.3}. Based on these facts, we can rule out the IRL as the cause of the contact resistance.

4.2 Se/Te-deficient Bi₂(Te_{0.9}Se_{0.1})_{3-δ}

It is well known that the intrinsic defects, such as vacancy and anti-site defect, in the rhombohedral structure M₂X₃ type (M=Sb, Bi; X=Te, Se) compounds play an important role in determining the electrical transport properties.²⁶⁻³¹ Since we did see a Te-deficient region at the thermoelectric material side in the Ni/Bi₂Te_{2.7}Se_{0.3} interface, we will discuss the possible defects that would determine the electrical transport properties near the contact interface. In a single crystal, the formation of metal anti-site defect M_X would be more energy-favorable than chalcogen vacancy V_X in the chalcogen-deficient Bi₂Te_{3-δ}.²⁶ The substitution of Bi with Sb would enhance the formation of M_X but suppress V_X, leading to more p-type behavior.²⁸ On the contrary, the replacement of Te with Se decreases the concentration of M_X and increases that of V_X, resulting in more n-type behavior.³⁰ In a polycrystalline M₂X₃, the dangling bonding due to missing chalcogen X behaves as partial V_X.¹² As a result, most Bi₂Te₃ and Bi₂Te_{3-x}Se_x polycrystals show a negative Seebeck coefficient. However, there is no systematic study about the impact of the significant deviation in M/X ratio from 2/3 even to the composition close to 1/1 in a poly nanocrystalline case. Fig. 8 shows the composition dependent electrical resistivity and Seebeck coefficient for the formula of Bi₂(Te_{0.9}Se_{0.1})_{3-δ}. When the M/X ratio is slightly deviated from stoichiometric value of 2/3 (δ<0.03), an increased electrical resistivity and Seebeck coefficient is seen in Bi₂(Te_{0.9}Se_{0.1})_{3-δ}. However, the electrical resistivity drops from 34 μΩ m to 14 μΩ m as the M/X ratio changes from δ=0.04 to δ=0.06. The high electrical resistivity due to the slight deviation from stoichiometric ratio could be one of the reasons for the high contact resistance we observed, but cannot be fully responsible since the resistivity is not so much higher and also such a layer is very thin due to the narrow composition.

4.3 Nickel doping effect

Nickel (Ni) diffused into the Bi₂Te₃-based thermoelectric element can act a dopant to affect the electrical transport properties. However, we lack the information about the most favorable atomic site for Ni in the Bi₂Te₃-type crystalline structure. In order to consider all the possibilities, including interstitial (Ni_i), and substitution at metallic site (Ni_M) and chalcogen site (Ni_X) in the M₂X₃ lattice, 1 at.% nickel was added into three Bi₂Te₃-based compounds: Ni_{0.01}Bi₂Te_{2.7}Se_{0.3}, Ni_{0.01}Bi_{1.99}Te_{2.7}Se_{0.3}, Bi₂Te_{2.7}Se_{0.29}Ni_{0.01}. All the samples were made by ball milling and hot pressing.

Fig. 9 shows the temperature dependent thermoelectric properties of the three Ni containing compounds. All three Ni containing samples show a high electrical resistivity (60~210 μΩ m) near room temperature, which is much higher than those of the nickel-free samples made by the same fabrication condition as shown in Fig. 9 (c). Furthermore, a positive Seebeck coefficient was seen in both Ni_{0.01}Bi₂Te_{2.7}Se_{0.3} and Bi₂Te_{2.7}Se_{0.29}Ni_{0.01}, which is in contrast to the normal negative Seebeck coefficient in Bi₂(Te_{0.9}Se_{0.1})_{3-δ} materials, as shown in Fig. 9 (d). In other words, Ni is a strong acceptor in this case. In order to get more information about the combined effect of the Ni doping and Te deficiency, more compositions in a map of χ and δ, according to the formula of (Bi_{1-χ}Ni_χ)₂(Te, Se)_{3-δ}, were investigated. Figure 10 shows that the contour map of electrical resistivity

and Seebeck coefficient for the $(\text{Bi}_{1-x}\text{Ni}_x)_2(\text{Te, Se})_{3-\delta}$ system at room temperature, which is built on 16 samples. It clearly shows a p-type region, corresponding to high resistivity. Very narrow p-type gap in chalcogen-deficiency (δ value) was seen in the Ni-free polycrystalline $\text{Bi}_2(\text{Te, Se})_{3-\delta}$. However, the p-type composition gap (δ value) significantly widens with increased nickel concentration as shown in Fig. 10 (c). As we discussed in section 4.2, the type of major carrier for $(\text{Bi}_{1-x}\text{Ni}_x)_2(\text{Te, Se})_{3-\delta}$ is a result of the competition between the metal antisite defect M_X and the chalcogen vacancy V_X . In the Ni-free case, M_X is dominant in a slightly chalcogen deficient sample, while V_X becomes dominant when the chalcogen deficiency is increased as illustrated in Fig. 10(d). In the Ni-containing situation, Ni plays a similar role with Bi as cation in the M_2X_3 ($\text{M}=\text{Bi, Ni}$ and $\text{X}=\text{Te, Se}$) structure. The formation energy of Ni_X could be even lower than Bi_X ($\text{X}=\text{Te, Se}$), explaining why a larger δ reverses the dominant defect from M_X to V_X , and hence a wider p-type composition region in δ value was seen in Ni containing $(\text{Bi}_{1-x}\text{Ni}_x)_2(\text{Te, Se})_{3-\delta}$. It is clear that the high contact resistance in n-type $\text{Ni}/\text{Bi}_2\text{Te}_{2.7}\text{Se}_{0.3}/\text{Ni}$ is caused by this highly resistive p-type composition region (PTR) due to Ni getting into the X-site and the chalcogen-deficiency. Regarding the diffusion of Ni into thermoelectric materials, the V_X due to chalcogen transferring towards the reaction interface could be another channel besides the grain boundary channel, and finally form some p-type defect Ni_X . Although the formation of Ni_X would neutralize the negative charged carrier and raise the electrical resistivity in n-type legs, it increases the positive charged carrier and reduces electrical resistivity in p-type legs. This is why we only see the high contact resistance in n-type legs not in p-type legs.

5. The Possible approaches to reduce the contact resistance

Based on the above findings, we tried to prevent the formation of the p-type region (PTR) within the Bi_2Te_3 -based thermoelectric element by adding two interlayers between Ni and $\text{Bi}_2\text{Te}_{2.7}\text{Se}_{0.3}$, to form a sandwich structure, i.e., $\text{Ni}/\text{Ni}_3\text{Te}_2/\text{Ni}_2\text{Te}_3/\text{Bi}_2\text{Te}_{2.7}\text{Se}_{0.3}/\text{Ni}_2\text{Te}_3/\text{Ni}_3\text{Te}_2/\text{Ni}$, and hot pressed at 500 °C. Fig. 11 shows the contact resistance measurement by the scanning probe measurement. The contact resistance is only $4 \mu\Omega \text{ cm}^2$, much lower though not low enough. However, the bonding strength of the sample is only ~11 MPa, which is understandable since there is no reaction to form the strong chemical bonding.

In order to balance the contact resistance and the bonding strength, we should allow some interface reaction without the formation of tellurium deficient region (TDR). The first thought was to introduce a $\text{Bi}_2\text{Te}_{2.7}\text{Se}_{0.3}$ barrier layer with extra chalcogen-containing compounds, such as Se, Te, and TeO_2 . However, the low melting point of pure Se and Te is problematic for hot pressing since it causes abnormal grain growth of $\text{Bi}_2\text{Te}_{2.7}\text{Se}_{0.3}$ at the interface during the hot press process, which weakens the bonding. NiSe_2 has a melting point of 856 °C, higher than that of Se, Te, and TeO_2 . A barrier layer (BL) made of 90% $\text{Bi}_2\text{Te}_{2.7}\text{Se}_{0.3}$ +10% NiSe_2 (BL-1) was tried and achieved a balanced bonding strength (16 MPa) and contact resistance ($9 \mu\Omega \text{ cm}^2$) in $\text{Ni}/\text{BL-1}/\text{Bi}_2\text{Te}_{2.7}\text{Se}_{0.3}/\text{BL-1}/\text{Ni}$, hot pressed at 425 °C, as shown in Fig. 12. However, these are not good enough for applications.

Another way was to use $\text{Bi}_2\text{Te}_{2.7}\text{Se}_{0.3}$ with 1% SbI_3 ($\rho < 5 \mu\Omega \text{ m}$) as the barrier layer, as shown in Fig. 12. No voltage jump was seen in the scanning voltage probe, i.e., no significant contact resistance ($< 1 \mu\Omega \text{ cm}^2$). The acceptor related to Ni_{Te} and Bi_{Te} could not create a p-type region due to its high n-type carrier provided by iodine. The significant reduction in contact resistance, confirmed our conclusion on high contact resistance in n-type Bi_2Te_3 legs. Furthermore, this hot pressed contact interface also shows enhanced bonding strength of 16 MPa as compared with that made by sputtering or electro-deposition methods (< 10 MPa). Although the bonding strength of as-fabricated n-type leg (16 MPa) is not strong as p-type leg (30 MPa), it does survive at least 10 thermal cycles between 220 °C and 20 °C.

Besides the Ni, some of other transition metals, such as Co, are also suggested for the metallization layer of n-type $\text{Bi}_2\text{Te}_{2.7}\text{Se}_{0.3}$.³¹⁻³³ It is reported that Co on $\text{Bi}_2(\text{Te, Se})_3$ shows significantly less diffusion, even at annealing temperatures at 200 °C.³² However, the contact made by directly hot pressing Co/ $\text{Bi}_2\text{Te}_{2.7}\text{Se}_{0.3}$ /Co layered powders at 500 °C has similar contact resistance ($\sim 200 \mu\Omega \text{ cm}^2$) with that in the case of Ni.

6. Conclusion

Nickel hot-pressed onto thermoelectric material shows a very strong bonding strength in both p-type Ni/ $\text{Bi}_{0.4}\text{Sb}_{1.6}\text{Te}_3$ /Ni (~ 30 MPa) and n-type Ni/ $\text{Bi}_2\text{Te}_{2.7}\text{Se}_{0.3}$ /Ni (~ 20 MPa). The good bonding strength was caused by the interface reaction. The major reaction product was Ni_3Te_2 for the Ni/ $\text{Bi}_{0.4}\text{Sb}_{1.6}\text{Te}_3$ interface, while NiTe for the Ni/ $\text{Bi}_2\text{Te}_{2.7}\text{Se}_{0.3}$. Since more Te element was consumed, a serious Te deficient region was identified at the interface of Ni/ $\text{Bi}_2\text{Te}_{2.7}\text{Se}_{0.3}$ but not in Ni/ $\text{Bi}_{0.4}\text{Sb}_{1.6}\text{Te}_3$. Furthermore, a fast diffusion of Ni into $\text{Bi}_2\text{Te}_{2.7}\text{Se}_{0.3}$ along the grain boundary was observed by TEM-EDS. With the doping effect of Ni, the p-type region is enlarged with δ value of chalcogen deficient $(\text{Bi}_{1-\gamma}\text{Ni}_\gamma)_2(\text{Te, Se})_{3-\delta}$. The combined effect of Te deficiency and Ni doping results in a wide p-type region, and consequently a high contact resistance in Ni/ $\text{Bi}_2\text{Te}_{2.7}\text{Se}_{0.3}$ /Ni ($R_c \sim 210 \mu\Omega \text{ cm}^2$, hot pressed at 500 °C), but not in the Ni/ $\text{Bi}_{0.4}\text{Sb}_{1.6}\text{Te}_3$ /Ni ($R_c < 1 \mu\Omega \text{ cm}^2$, hot pressed at 500 °C). The high contact resistance in Ni/ $\text{Bi}_2\text{Te}_{2.7}\text{Se}_{0.3}$ /Ni was significantly reduced by a few different approaches. Among the approaches, a low contact resistance ($< 1 \mu\Omega \text{ cm}^2$) combined with enhanced bonding strength (16 MPa) is obtained by adding a barrier layer between Ni and $\text{Bi}_2\text{Te}_{2.7}\text{Se}_{0.3}$ to neutralize the acceptor center generated from the interface reaction.

Acknowledgement

This work is supported by “Solid State Solar-Thermal Energy Conversion Center (S3TEC)”, an Energy Frontier Research Center funded by the U.S. Department of Energy, Office of Science, Office of Basic Energy Science under award number DE-SC0001299/DE-FG02-09ER46577 (GC and ZFR).

References

1. G. L. Bennett, *Space applications*, in *CRC Handbook of Thermoelectrics*, edited by D. M. Rowe, CRC Press, Boca Raton, 1995.
2. T. Kajikawa, Thermoelectric power generation system recovering industrial waste heat, in *CRC Handbook of Thermoelectrics* edited by D. M. Rowe, Taylor & Francis Group, Boca Raton, 2006.
3. K. Matsubara and M. Matsuura, A thermoelectric application to vehicles, in *CRC Handbook of Thermoelectrics* edited by D. M. Rowe, Taylor & Francis Group, Boca Raton, 2006.
4. H. J. Goldsmid, *J. Appl. Phys.*, 1961, 32, 2198-2202.
5. H. Scherrer and S. Scherrer, Bismuth telluride, antimony telluride, and their solid solutions, in *CRC Handbook of Thermoelectrics* edited by D. M. Rowe, CRC Press, Boca Raton, 1995.
6. B. Poudel, Q. Hao, Y. Ma, Y. C. Lan, A. Minnich, B. Yu, X. Yan, D. Z. Wang, A. Muto, D. Vashaee, X. Y. Chen, J. M. Liu, M. S. Dresselhaus, G. Chen and Z. F. Ren, *Science*, 2008, **320**, 634-638.
7. Y. Ma, Q. Hao, B. Poudel, Y. C. Lan, B. Yu, D. Z. Wang, G. Chen and Z. F. Ren, *Nano Lett.*, 2008, **8**, 2580-2584.
8. L. D. Zhao, B. P. Zhang, J. F. Li, M. Zhou, W. S. Liu and J. Liu, *J. Alloys Compounds*, 2008, **455**, 259-264.
9. L. D. Zhao, B. P. Zhang, W. S. Liu and J. F. Li, *J. Appl. Phys.*, 2009, **105**, 023704.

10. X. Yan, B. Poudel, Y. Ma, W. S. Liu, G. Joshi, H. Wang, Y. C. Lan, D. Z. Wang, G. Chen and Z. F. Ren, *Nano Lett.*, 2010, **10**, 3373-3378.
11. W. J. Xie, J. He, H. J. Kang, X. F. Tang, S. Zhu, M. Laver, S. Y. Wang, J. R. D. Copley, C. M. Brown, Q. J. Zhang and T. M. Tritt, *Nano Lett.*, 2010, **10**, 3283-3289.
12. W. S. Liu, Q. Y. Zhang, Y. C. Lan, S. Chen, X. Yan, Q. Zhang, H. Wang, D. Z. Wang, G. Chen and Z. F. Ren, *Adv. Energy Mater.*, 2011, **1**, 577-587.
13. W. S. Liu, K. C. Lukas, K. McEnaney, S. Lee, Q. Zhang, C. P. Opeil, G. Chen and Z. F. Ren, *Energy Environ. Sci.*, 2013, **6**, 552-560.
14. D. Kraemer, B. Poudel, H. P. Feng, J. C. Caylor, B. Yu, X. Yan, Y. Ma, X. W. Wang, D. Z. Wang, A. Muto, K. McEnaney, M. Chiesa, Z. F. Ren and G. Chen, *Nat. Mater.*, 2012, **10**, 532-538.
15. K. McEnaney, D. Kraemer, Z. F. Ren and G. Chen, *J. Appl. Phys.*, 2012, **110**, 074502.
16. R. O. Carlson, *J. Phys. Chem. Solids*, 1960, **13**, 65.
17. S. Fujimoto, S. Sano and T. Kajitani, *Jpn. J. Appl. Phys.: Part 1*, 2007, **46**, 5033.
18. I. V. Gasenkova and T. E. Svechnikova, *Inorg. Mater.*, 2004, **40**, 570-575.
19. T. Y. Lin, C. N. Liao and A. T. Wu, *J. Electron. Mater.*, 2012, **41**, 153-158.
20. S. P. Sheng, J. Yang, B. Poudel, B. Yu, Y. H. Chang, Z. F. Ren and G. Chen, *Phys. Chem. Chem. Phys.*, 2013, **15**, 6757.
21. K. Xiong, W. Wang, H. N. Alshareef, R. P. Gupta, J. B. White, B. E. Gnade and K. Cho, *J. Phys. D: Appl. Phys.*, 2010, **43**, 115303.
22. Y. C. Lan, G. Wang, G. Chen and Z. F. Ren, *Appl. Phys. Lett.* 2008, **92**, 101910.
23. O. D. Lyore, T. H. Lee, R. P. Gupta, J. B. White, H. N. Alshareef, M. J. Kim and B. E. Gnade, *Surface and Interface Analysis*, 2009, **41**, 440-444.
24. Ni₂SbTe: PDF #01-089-7153.
25. S. N. Zhevnenko, D. V. Vaganov and E. I. Gershman, *J. Mater. Sci.*, 2011, **46**, 4248-4253.
26. D. O. Scanlon, P. D. C. King, R. P. Singh, A. de la Torre, S. M. Walker, G. Balakrishnan, F. Baumberger and C. R. A. Catlow, *Adv. Mater.*, 2012, **24**, 2154-2158.
27. J. M. Schultz, J. P. McHugh and W. A. Tiller, *J. Appl. Phys.*, 1962, **33**, 2443-2450.
28. Z. Sary, J. Horay, M. Stordeur and M. S Tolzer, *J. Phys. Chem. Solids*, 1988, **49**, 29-34.
29. J. Horak, J. Navratil and Z. Sary, *J. Phys. Chem. Solids*, 1992, **53**, 1067-1072.
30. P. Lostak, C. Drasar, D. Bachan, L. Benes and A. Krejcova, *Radiation effects & defects in solids: incorporating plasma science & plasma technology*, 2010, **165**, 211-215.
31. K. C. Lukas, W. S. Liu, Z. F. Ren, C. P. Opeil, *J. Appl. Phys.*, 2010, 112, 054509.
32. R. P. Gupta, O. D. Lyore, K. Xiong, J. B. White, Kyeongjae Cho, H. N. Alshareef and B. E. Gnade, *Electrochem. Solid-State Lett.*, **2009**, 12, H395-H397.
33. K. Xiong, W. C. Wang, H. N. Alshareef, R. P. Gupta, J. B. White, B. E. Gnade and K. Cho, *J. Phys. D.: Appl. Phys.*, **2010**, 43, 115303.

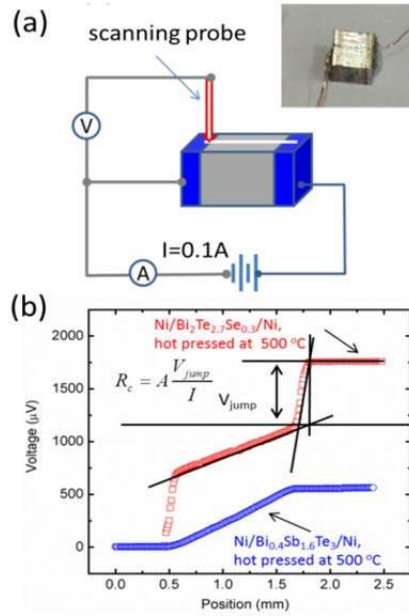


Fig. 1 Schematic diagram of a scanning voltage probe for contact resistance measurement, and a Bi_2Te_3 -based leg (inset); (b) contact resistance measurement for both n-type $\text{Ni}/\text{Bi}_2\text{Te}_{2.7}\text{Se}_{0.3}/\text{Ni}$ and p-type $\text{Ni}/\text{Bi}_{0.4}\text{Sb}_{1.6}\text{Te}_3/\text{Ni}$. The contact resistance was determined from the averaged voltage jump, where cross-section of the thermoelectric element is $A = 1.8 \times 1.8 \text{ mm}^2$ and electrical current is $I = 0.1 \text{ A}$.

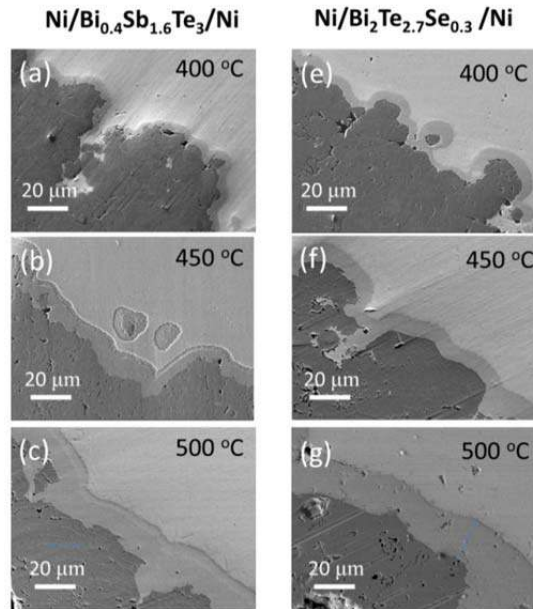


Fig. 2 Microstructure of contact interface made by directly hot pressing the Ni powders and TE powders together, (a) $\text{Ni}/\text{BiSbTe}/\text{Ni}$, hot pressed at $400 \text{ }^\circ\text{C}$; (b) $\text{Ni}/\text{BiSbTe}/\text{Ni}$, hot pressed at $450 \text{ }^\circ\text{C}$; (c) $\text{Ni}/\text{BiSbTe}/\text{Ni}$, hot pressed at $500 \text{ }^\circ\text{C}$; (e) $\text{Ni}/\text{BiTeSe}/\text{Ni}$, hot pressed at $400 \text{ }^\circ\text{C}$; (f) $\text{Ni}/\text{BiTeSe}/\text{Ni}$, hot pressed at $450 \text{ }^\circ\text{C}$; (g) $\text{Ni}/\text{BiTeSe}/\text{Ni}$, hot pressed at $500 \text{ }^\circ\text{C}$. The dark region is nickel element, and the light region is thermoelectric element. BiSbTe : $\text{Bi}_{0.4}\text{Sb}_{1.6}\text{Te}_3$, BiTeSe : $\text{Bi}_2\text{Te}_{2.7}\text{Se}_{0.3}$.

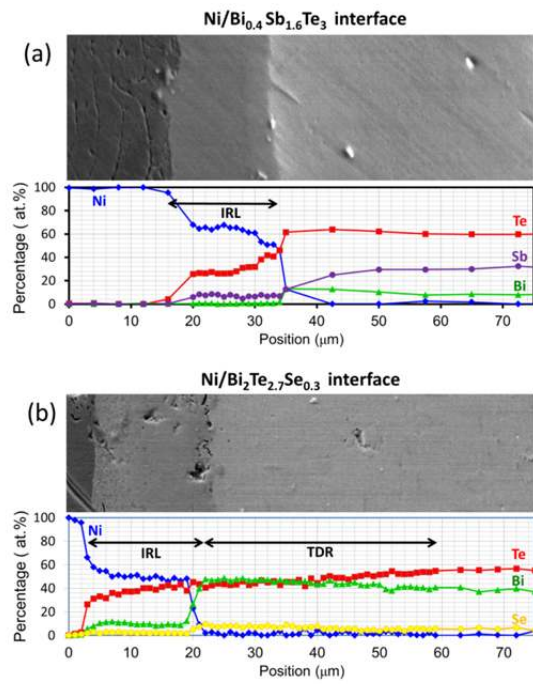


Fig. 3 Comparison of composition profile between (a) Ni/Bi_{0.4}Sb_{1.6}Te₃ interface and (b) Ni/Bi₂Te_{2.7}Se_{0.3} interface obtained from selected area SEM-EDS. IRL: interface reaction layer, TDR: Te-deficient region.

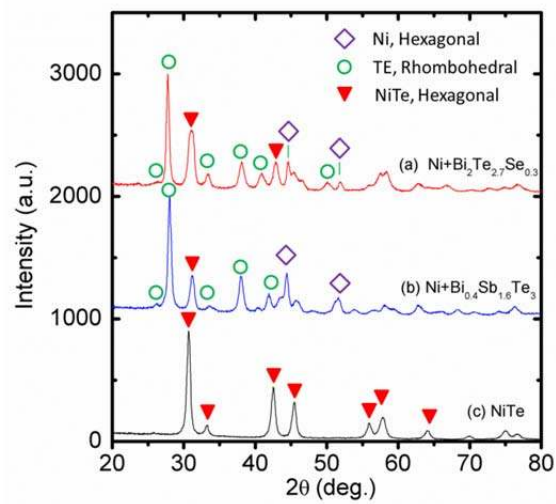


Fig. 4 XRD spectra of Ni+Bi₂Te_{2.7}Se_{0.3} (20 wt.% Ni), Ni+Bi_{0.4}Sb_{1.6}Te₃ (20 wt.% Ni), and NiTe.

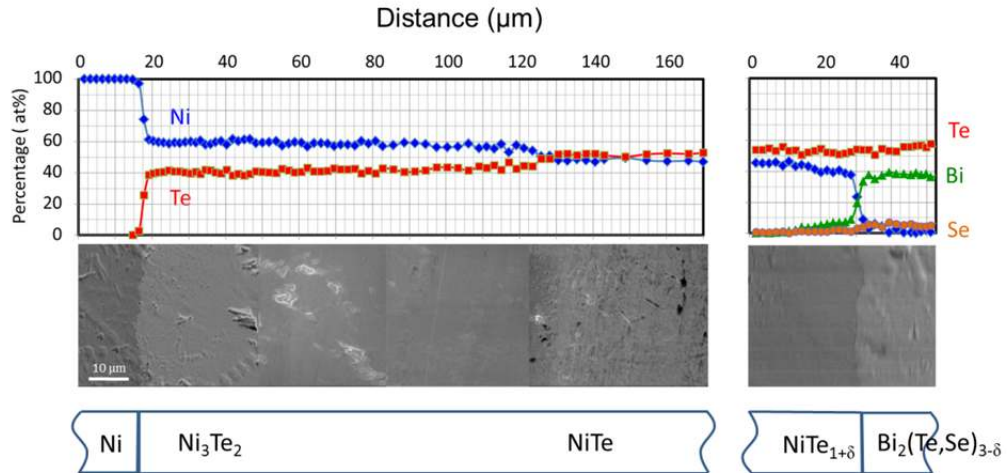


Fig.5 Composition profile of Ni/NiTe/Bi₂Te_{2.7}Se_{0.3}, made by directly hot pressing at 500 °C for 2 min

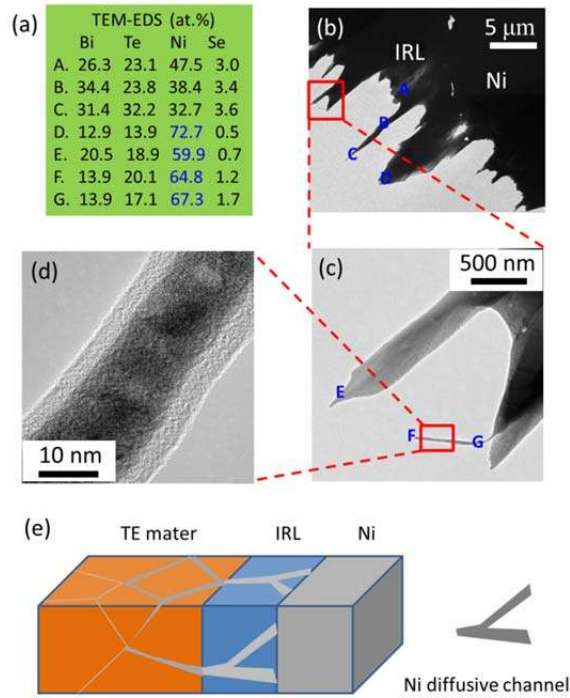


Fig. 6 (a) Composition of selected interesting points (A-G) by TEM-EDS, (b-d) the typical TEM image of the Ni/Bi₂Te_{2.7}Se_{0.3} interface, (e) a schematic model for the fast diffuse of Ni along the grain boundary.

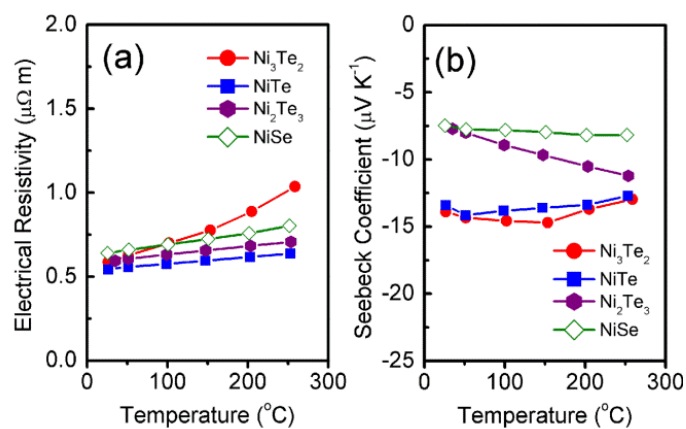


Fig. 7 Temperature dependent electrical resistivity and Seebeck coefficient of Ni_3Te_2 , NiTe , Ni_2Te_3 , and NiSe .

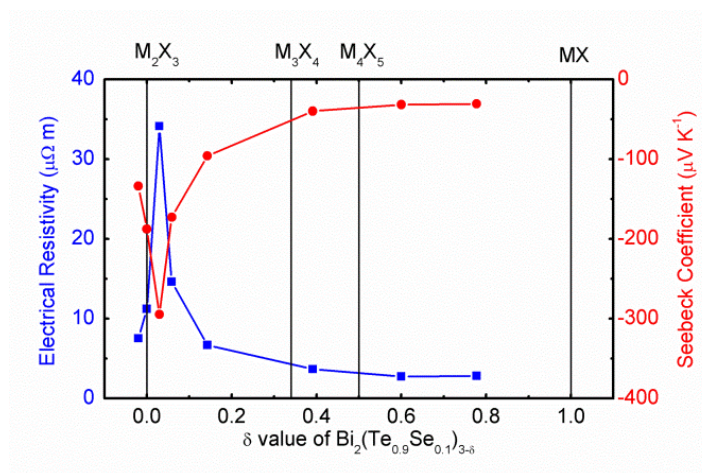
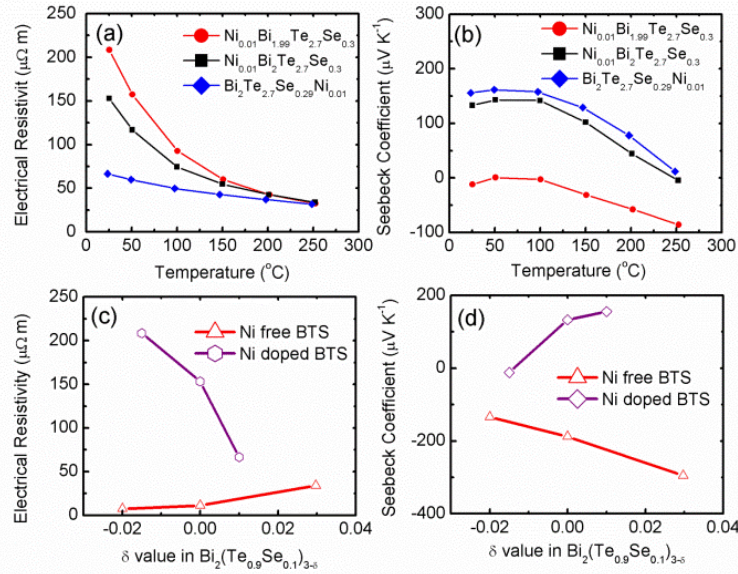


Fig. 8 Electrical resistivity and Seebeck coefficient of $\text{Bi}_2(\text{Te}_{0.9}\text{Se}_{0.1})_{3-\delta}$ compounds made by ball milling and hot pressing as function of the value of δ .



FFig 9 Temperature dependent electrical resistivity (a) and Seebeck coefficient (b) for the Ni containing Bi₂Te₃-based compounds: Ni_{0.01}Bi₂Te_{2.7}Se_{0.3}, Ni_{0.01}Bi_{1.99}Te_{2.7}Se_{0.3}, and Bi₂Te_{2.7}Se_{0.29}Ni_{0.01}. Composition dependent electrical resistivity (c) and Seebeck coefficient (d) for Ni free and Ni containing Bi₂(Te_{0.9}Se_{0.1})_{3- δ} .

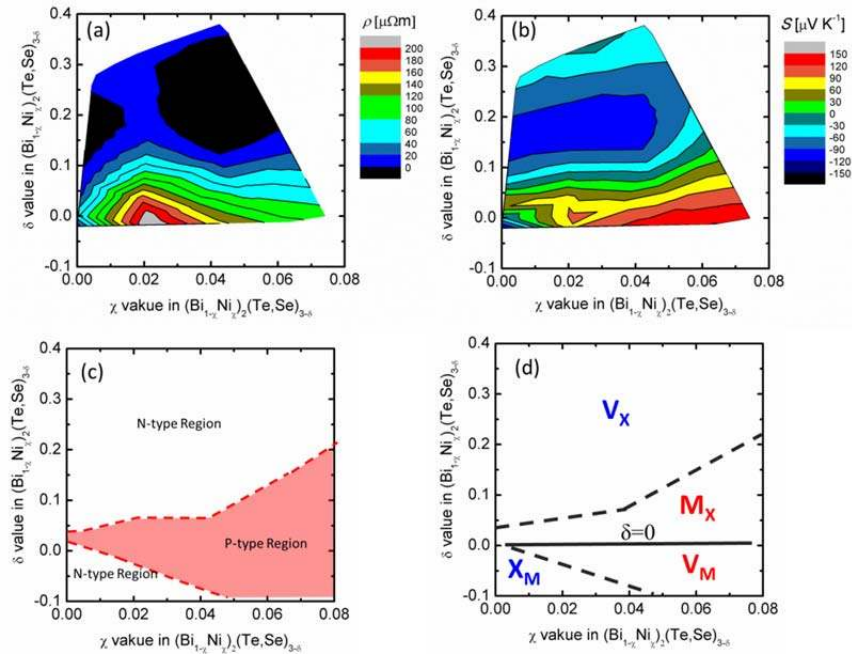


Figure 10, Contour map of electrical resistivity (a) and Seebeck coefficient (b) for the $(\text{Bi}_{1-x}\text{Ni}_x)_2(\text{Te,Se})_{3-\delta}$ system at room temperature, (c) the major carrier map, and (d) the major defect map.

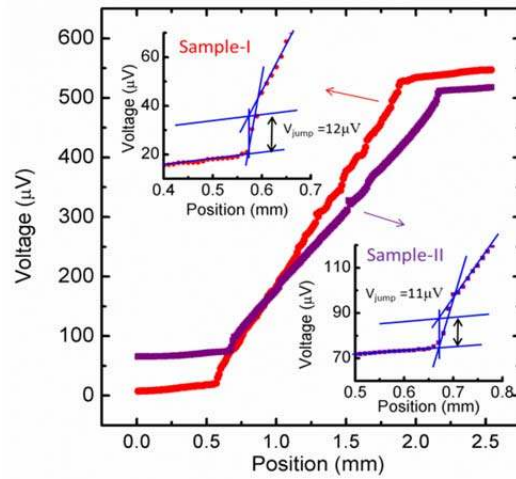


Fig.11 Contact resistance measurement by the scanning probe for two Ni/Ni₃Te₂/Ni₂Te₃/Bi₂Te_{2.7}Se_{0.3}/Ni₂Te₃/Ni₃Te₂/Ni legs, which is made by hot pressing at 500 °C. The cross section of the leg is 1.8 x 1.8 mm², the current is 0.1 A.

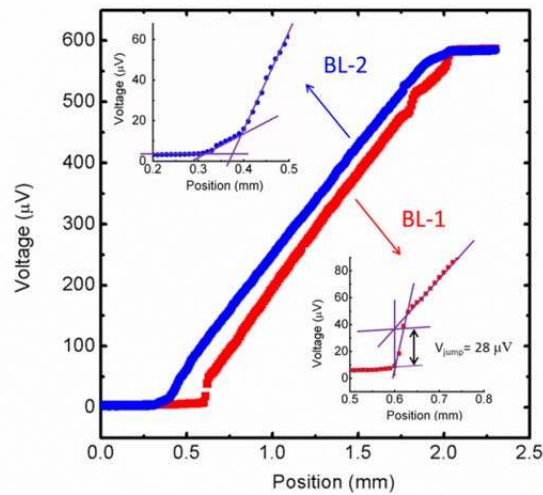


Fig. 12 Contact resistance measurement by the scanning probe for two n-type legs with barrier layers (BL): Ni/BL-1/ Bi₂Te_{2.7}Se_{0.3}/ BL-1/Ni and Ni/BL-2/ Bi₂Te_{2.7}Se_{0.3}/ BL-2/Ni, which is made by hot pressing at 425 °C. BL-1: 90% Bi₂Te_{2.7}Se_{0.3}+10% NiSe₂, BL-2: 1% SbI₃ doped Bi₂Te_{2.7}Se_{0.3}.